A Letters Journal Exploring the Frontiers of Physics

October 2011

EPL, **96** (2011) 14001 www.epljournal.org
doi: 10.1209/0295-5075/96/14001

Vibration-induced slip in sheared granular layers and the micromechanics of dynamic earthquake triggering

M. Griffa[1(a)], E. G. Daub[2,3], R. A. Guyer[2], P. A. Johnson[2], C. Marone[4,5] and J. Carmeliet[1,6]

[1] *Laboratory for Building Science and Technology, Swiss Federal Laboratories for Materials Science and Technology, EMPA - Überlandstrasse 129, CH-8600, Dübendorf, Switzerland*
[2] *Solid Earth Geophysics Group, Los Alamos National Laboratory - MS D443, NM 87545, Los Alamos, USA*
[3] *Center for Nonlinear Studies, Los Alamos National Laboratory - MS B258, NM 87545, Los Alamos, USA*
[4] *Department of Geosciences, Pennsylvania State University - PA 16802, State College, USA*
[5] *G3 Center and Energy Institute, Pennsylvania State University - PA 16802, State College, USA*
[6] *Chair of Building Physics, Swiss Federal Institute of Technology in Zürich, ETHZ - CH-8093, Zürich, Switzerland*

received 13 February 2011; accepted in final form 11 August 2011
published online 15 September 2011

PACS 45.70.-n – Granular systems
PACS 61.43.-j – Disordered solids
PACS 91.30.Px – Earthquakes

Abstract – We perform 2D Molecular Dynamics simulations of sheared granular layers in the presence of applied vibration. A primary goal is to understand the physics of dynamic earthquake triggering. We adopt a mesoscopic measure of non-affine deformation for characterizing the granular dynamics during slip without or with applied vibration. Our results show that the onset of non-affine strains correlates with the onset of slip and appears earlier in the presence of vibration than in its absence, in agreement with the evidence for triggered slip.

Introduction. – When the seismic waves broadcast from the moment magnitude $M_w = 7.9$ Denali earthquake (Alaska) washed over the western US, they induced a notable increase in seismicity [1]. Dynamic triggering of one earthquake via the seismic waves radiated by a remote, second earthquake is a phenomenon first recognized in the early 1990's [2,3]. Triggering offers important clues about the physics of tectonic fault slip and earthquakes. A key component in the physics of triggering is the fault gouge, a granular system derived from wear of the tectonic plates moving past one another [4].

In order to investigate the role that fault gouge plays in earthquake instabilities, laboratory experiments focusing on stick-slip of granular materials are often used as an analog for earthquake failure. Marone and collaborators have developed a double-axial experimental setup for manipulating sheared granular layers in order to mimic many types of fault-related seismic events, *e.g.*, continuous sliding, intermittent stick-slip, quasi-periodic stick-slip [5–7]. Using this apparatus, Johnson *et al.* found that a laboratory analogue of earthquakes could be triggered upon subjecting the granular layers to transient sound vibration [8].

Here we introduce a 2D Molecular Dynamics (MD) model of a sheared granular system that allows us to study dynamic triggering. A primary advantage in MD simulations is the access to the particle-scale variables, in contrast to most laboratory experiments. MD simulations provide the means to characterize the granular dynamics underlying stick-slip and dynamic triggering, the principal objectives of our work.

Simulation approach. – A full, detailed presentation of the model is available online in the Supplementary Materials that can be downloaded from one of the authors' web site, clicking on this link[1]. We present here only the most relevant features. Each reported variable/parameter is non-dimensional, expressed in basic dimensional units $L_0 = 1.5 \cdot 10^{-4}$ m, $t_0 = 1$ s and $M_0 = 1$ kg, respectively for length, time and mass. The largest particle in the model has radius equal to 1.

Figure 1(a) shows a section of our 2D MD numerical model for a sheared fault gouge layer. The model schematically consists of a driving block, a granular system, and a substrate block.

(a) E-mail: michele.griffa@empa.ch

[1] http://www.calcolodistr.altervista.org/en/work/Preprints_en.html.

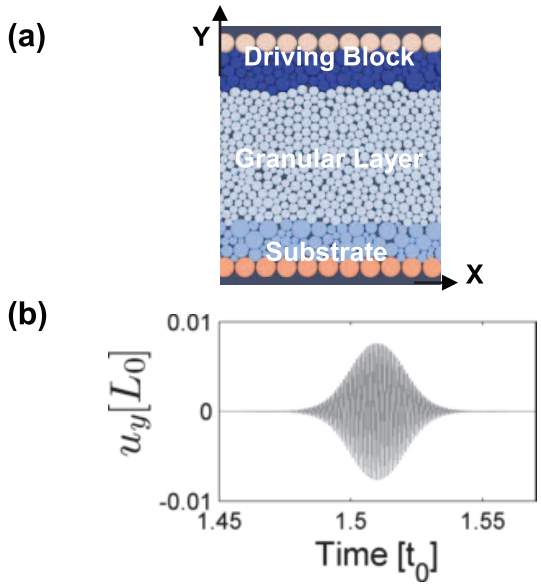

Fig. 1: (Color online) (a) MD model comprised of the driving block (top), the granular layer (center) and the substrate block (bottom). A constant normal load is applied in the Y direction, while periodic boundary conditions are imposed in the X direction. A shear load is applied in the X direction, from left to right, by imposing a constant displacement rate $V_{X,0}$ on the top of the driving block. The particles are colored in order to distinguish different components of the model. (b) Time history of the substrate's bottom displacement imposed in the Y direction, u_y, in order to apply vibration to the system. Notice the small peak-to-peak amplitude ≈ 0.015.

The driving block, fig. 1(a) top, is a structured, elastic material comprised of bonded poly-disperse 2D disks that interact among themselves with compressional, shear, and bending forces [9,10]. This block is driven by assigning the same velocity in the X direction, $V_{X,0}$, to the top layer particles (uniform set of large particles). The imposed velocity applies a shear load to the granular system. The substrate block is essentially the same as the driving block. Its bottom layer (uniform set of large particles) is fixed in X. The driving block/substrate has a thickness of approximately 3.5. The driving block and substrate are meant to represent simplified models of both laboratory and tectonic sheared systems.

The granular system is a collection of unbonded, poly-disperse particles that interact among themselves and with driving block/substrate particles via contact, frictional forces. These forces have normal and shear components represented by linear contact mechanics laws [9]. The granular layer represents the fault gouge, the wear material within a tectonic fault. It is held between the driving block and the substrate block, within a region approximately 12 units thick, by imposing a normal load $\sigma_n = 600 \approx 4\,\mathrm{MPa}$. At the beginning of each simulation, the granular system undergoes a consolidation stage. During the consolidation stage, the top of the driving block and bottom of substrate are displaced vertically until they exert the desired normal stress, σ_n, on the granular layer. Following compaction, we allow the Y thickness of the system to reach a steady state. Finally, once the system has reached a steady thickness, the shear load is applied. While shear is imposed, the top of the driving block is displaced in Y in a servo-controlled fashion, to keep the normal load equal to σ_n. The bottom of the substrate remains fixed in Y at the steady-state position, except during the short time intervals when AC vibration is imposed as a Y displacement, as in the simulations by Capozza *et al.* [11]. It follows that the normal stress on the top of the driving block is constant and equal to σ_n while the one on the bottom of the substrate fluctuates about σ_n with an amplitude of a few percent of σ_n (see the Supplementary Materials for additional details in footnote [1]). This implementation allows for more accurate control of the applied vibration. However, it limits the range of investigation to small vibration amplitudes, which is the case here addressed.

The overall system has a length of 70 in X. Periodic boundary conditions are applied in the X direction in order to reduce the computation time. The granular layer particle sizes, shapes, and the boundary normal load are selected to agree with those of the laboratory apparatus used in the experimental studies of triggered stick-slip [8].

This model has two important ingredients designed to mimic aspects of the laboratory apparatus and natural faults. The first of these is the distribution of roughness at the boundary of the granular shear zone, given by the polydispersivity of the bonded particles. The second relevant ingredient is the spatial extension and deformability of the driving block/substrate.

A spectrum of surface roughness scales is a necessary feature for accurate simulation of granular stick-slip, for two reasons. First, field measurements of fault surface roughness indicate that the roughness spectrum spans many orders of magnitude [12] and plays a critical role in determining the highly heterogeneous stress and displacement fields in the near field of the fault surface [13]. Second, laboratory experiments under geophysical stresses show that fault surface roughness can promote stick-slip dynamics by increasing the coupling between boundary blocks and granular layer and decreasing boundary slip. A granular layer can exhibit stable sliding if sheared between smooth surfaces, but shows stick-slip if the surfaces are rough [6].

The finite size and deformability of the driving block/substrate is the second important ingredient of our model. The complexity of earthquakes on mature faults is due to complicated interactions between local deformations in the granular gouge and deformable elastic rocks in the Earth's crust. Our model accounts for this aspect of natural faults by shearing the granular material between two deformable and spatially extended blocks. This feature represents a key difference compared to spring-slider models of boundary blocks in MD shear setups [14–16]. These models usually consider the driving

block as a rigid body, made of only one layer of constant size particles bonded to each other.

The control parameters $(\sigma_n, V_{X,0})$ were chosen in order to drive the system in a quasi-periodic stick-slip regime. We report results from a typical example of two runs that allow us to study details of dynamic-wave triggering. Both runs start from the same initial state. In the first run, the reference run, the driving block is driven at $V_{X,0} = 4$ out to times where there is steady, quasi-periodic, stick-slip behavior. In the second run, the perturbed run, the driving block is driven as in the reference run and in addition a transient AC vibration is applied. This vibration is a Y displacement, u_y, of the substrate block bottom layer at frequency 10^3, within a Gaussian window, during the time interval $[1.46; 1.56]$, fig. 1(b). The Gaussian envelope is applied to conduct a preliminary investigation of the role of vibration amplitude in dynamic triggering, shown to be amplitude dependent both in the laboratory [7] and in the Earth [17]. A detailed parametric study addressing the consequences of AC vibration timing, peak amplitude and frequency is part of a more extensive ongoing study.

Results. – We monitor three macroscopic variables continuously throughout both runs: the Center-Of-Mass (COM) velocity of the driving block, $\bar{V}$, the system thickness in the Y direction (distance from bottom of substrate block to top of driving block), T, and the friction coefficient, μ_f (the ratio of the total shear stress on the driving block, τ, to the average normal confining stress, σ_n). Figures 2(a)–(d) show, respectively, the X-component of the driving block's COM velocity, V_X, normalized by $V_{X,0}$, $\tilde{V}_X \equiv \frac{V_X}{V_{X,0}}$, the thickness T, the substrate's bottom displacement in Y, u_y, for the perturbed run, as in fig. 1(b), and the friction coefficient μ_f. Black solid lines refer to the reference run while gray solid lines to the perturbed run.

The driving block/granular layer coupled dynamics shown in fig. 2 is representative of what we observe during a long series of successive stick-slip events, both with and without applied vibration. Figure S1 of the Supplementary Materials (see footnote [1]) shows, for example, $\tilde{V}_X$, T and μ_f for another time interval, $[10.06; 10.75]$, with similar type of transient AC displacement applied in the time interval $[10.06; 10.16]$. We have analyzed 225 stick-slip events for both the reference and the perturbed run.

Reference run. During the reference run, the driving block moves at an average speed V_X less than the loading velocity $V_{X,0}$, causing the friction coefficient to increase steadily. We call these time intervals of shear stress accumulation "stick periods". Note that the driving block does not physically stick during these time intervals, though the shear stress increases because the driving block lags behind the load velocity ($\tilde{V}_X < 1$). This type of behavior is also typical of experiments using the double-axial shear configuration. Examples of stick periods in fig. 2(d) are the time intervals $I_1 = [1.460; 1.537]$, $I_2 = [1.548; 1.570]$, $I_3 = [1.588; 1.639]$, $I_4 = [1.659; 1.826]$ and $I_5 = [1.840; 1.872]$. During these periods, the average value of $\tilde{V}_X$ is 0.8646, 0.8532, 0.7719, 0.878 and 0.9492, respectively. Similar values are achieved during other stick periods of the reference run. Following each stick phase there is a slip phase, when the COM speed abruptly increases in amplitude while the friction coefficient drops. This sudden increase in the COM speed and sudden

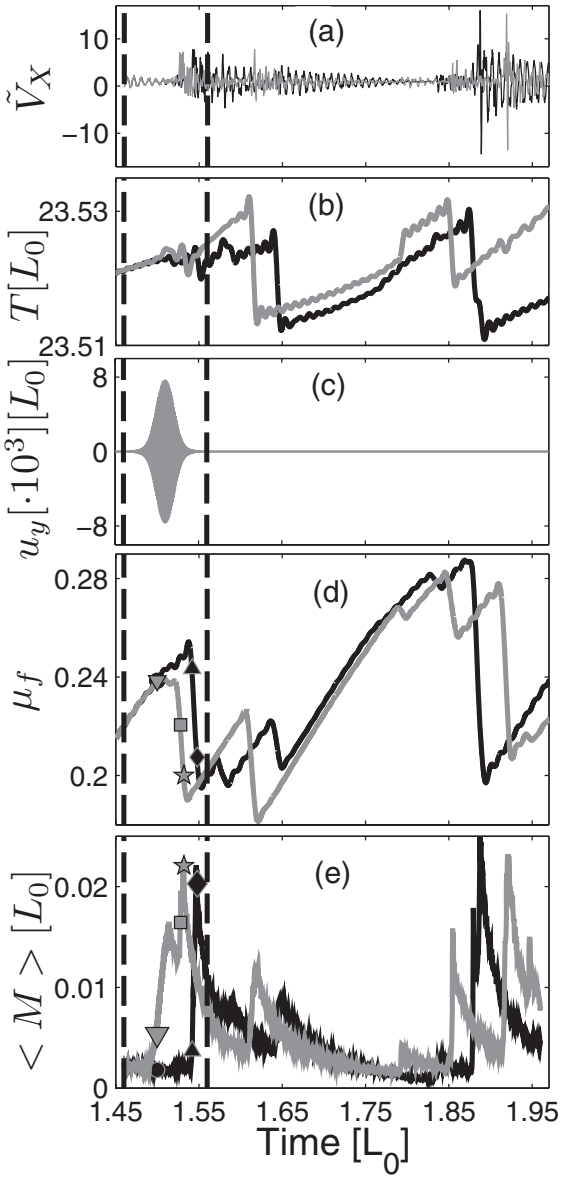

Fig. 2: Macroscopic signals. (a) Driving block's (normalized) Center-Of-Mass (COM) velocity in the shear direction (X), $\tilde{V}_X$. (b) Model's thickness in Y direction, T. (c) Substrate's bottom displacement in Y direction, u_y, for the perturbed run. (d) Coefficient of friction, μ_f. Symbols are defined in fig. 3. (e) Granular layer ensemble average ($\langle\cdot\rangle$) of the non-affine deformation metric M. The vertical dashed lines in all the insets outline the time interval of interest, when vibration is imposed during the perturbed run. In all plots, black lines refer to the reference run (without applied vibration), and gray lines refer to the perturbed run (with applied vibration).

decrease in the friction coefficient signals the decoupling of driving block and granular system, that accompanies slip.

During time intervals of steady friction coefficient increase, *e.g.*, during $[1.460; 1.537]$ and $[1.65; 1.80]$, the granular system undergoes Reynolds' dilatancy [18], fig. 2(b). When a slip event occurs, there is usually, but not always, an associated compaction of the granular layer. In the catalog of 225 slip events, 155 of them (68.9%) occured with compaction. For example, the slip event within the time interval $[1.46; 1.56]$ shown in fig. 2(d) happens with almost no change in T (no compaction) while most of the following slips are accompanied by compaction. A quantitative analysis of the overall series of 155 slip events accompanied by compaction shows that there is weak correlation between the size of the friction coefficient drop during slip, $|\Delta\mu_f|$, and the size of the thickness change within the same slip time interval, $|\Delta T|$. The linear correlation coefficient between the two variables is in this case $R = 0.5109$. See the Supplementary Materials in footnote [1] for detailed analysis. The degree of correlation between $|\Delta\mu_f|$ and $|\Delta T|$ is a typical feature for our simulated stick-slip dynamics and is consistent with the high degree of irregularity and broad size distribution of our slip events, quantified by the Cumulative Distribution Function (CDF) of $|\Delta\mu_f|$, also presented in the Supplementary Materials (see footnote [1]).

To bridge the macroscopic scale information, provided by the friction coefficient signals, with information at the granular scale we use a metric function, M. The metric function M identifies where the strain fields are strongly, spatially non-uniform, at a mesoscopic scale [19–21]. We are interested in highlighting the highly irreversible (plastic) particle rearrangements that are necessary to permit localized granular flow. This metric function provides at each time t an estimate of the local amount of cumulative, spatially non-uniform, deformation occuring within the time interval $[t; t^* = t + \Delta t]$ in the neighborhood of each particle. It relies upon the idea that each strain tensor field, $\bar{\bar{\epsilon}}(\bar{r}, t)$, associated with the deformation within that temporal interval, can be locally decomposed into two parts, a spatially uniform component, $\bar{\bar{\epsilon}}^A$, corresponding to the affine mapping matrix $\bar{\bar{A}}$, $\bar{\bar{\epsilon}}^A = \bar{\bar{A}} - \bar{\bar{1}}$, where $\bar{\bar{1}}$ is the identity matrix, and a non-affine, *i.e.*, spatially varying, one. For each particle i, the neighborhood is defined as a circle centered at the particle and with radius L. The position $\bar{r}^c$ (relative to the circle's center of mass) of each particle c, belonging to that neighborhood, is recorded at time t and t^*. The matrix $\bar{\bar{A}}(t, t^*)$ can be estimated by minimization of the least square objective function $f_i(\bar{\bar{A}}(t, t^*)) \equiv \sum_c \|\bar{r}^c(t^*) - \bar{r}^{c,A}(t^*)\|^2$ [19]. The vector $\bar{r}^{c,A}(t^*) \equiv \bar{\bar{A}}(t, t^*) \cdot \bar{r}^c(t)$ would be the particle position at time t^* if the strain were purely affine. The square root of the minimum value of f_i, called M_i, is thus a function of particle position and time, $M(\bar{r}, t)$, and provides an estimate of the amount of non-affine deformation in the neighborhood of each particle. We choose $\Delta t = 2.5 \cdot 10^{-4}$, a value that is large enough to capture even small particle rearrangements, *e.g.*, due to rotations, but is small compared to the granular flow time scale. We also choose $L = 2.2$, such that each particle neighborhood provides enough spatial resolution for highly localized deformation but contains a sufficient number of particles (on average 20) [20].

Figure 2(e), black line, shows the granular layer ensemble average value of M, $\langle M \rangle(t)$, *vs.* time. For each slip event, $\langle M \rangle(t)$ clearly illustrates that the onset of macroscopic slip (fig. 2(d)) is associated with a sudden increase in the average non-affine deformation level inside the granular layer. The maximum value of $\langle M \rangle(t)$ occurs when the friction coefficient is at its minimum value (end of slip). The subsequent stick period is accompanied by a slow decay (recovery) of $\langle M \rangle(t)$ to the ambient level. These results demonstrate that $\langle M \rangle(t)$ is a mesoscopic "fingerprint" for the onset/end of the localized particle rearrangement during granular stick-slip dynamics. It means that a locally non-uniform strain tensor field develops during the slip event, in agreement with the Shear Transformation Zone theory [22,23].

Figure 3, left column, shows three snapshots of $M(\bar{r}, t)$ at different time instants t_i during the corresponding stick-slip cycle. Figure 3(a) shows that before the onset of slip, a small number of very localized regions exhibits very low levels of non-affine deformation (note the logarithmic color scale). These regions are primarily due to single particles acting like rattlers (particles trapped into an area of relatively high free volume) and/or more coherent structures like vortexes, as observed in biaxial compression simulations [24]. Rapid slip is accompanied by a steep increase in the non-affine deformation, fig. 3(c): the peak values of M occur only within a shallow layer, corresponding to the shear zone. However, our simulation also shows that non-affine deformation spreads within the bulk of the granular layer at later times during the slip event (see fig. 3(e) and the Supplementary Materials in footnote [1]).

Perturbed run. Up to this point we have focused on the reference run. We now consider the effect of the applied AC displacement. The perturbing AC vibration is on during the time interval bracketed by the dashed lines, $[1.46; 1.56]$. Figure 2(a), gray line, shows that $\tilde{V}_X$, still fluctuates about an average value similar to the one in the reference run. During the five stick periods that can be recognized in fig. 2(d), *i.e.*, the time intervals $\tilde{I}_1 = [1.460; 1.500]$, $\tilde{I}_2 = [1.534; 1.605]$, $\tilde{I}_3 = [1.624; 1.789]$, $\tilde{I}_4 = [1.799; 1.842]$ and $\tilde{I}_5 = [1.861; 1.911]$, $\tilde{V}_X$ has an average value equal to 0.8913, 0.8326, 0.8529, 0.9177 and 0.8560, respectively. Similar values are seen during following stick periods.

The main effect of the AC vibration within $[1.46; 1.56]$ is to trigger slip at a lower shear stress level, compared to the reference run. The slip initiates at about time $t = 1.508$, very close to the maximum of the AC vibration (see fig. 2(c)). A similar result can be observed in fig. S1 of the Supplementary Materials (see footnote [1]) for AC vibration

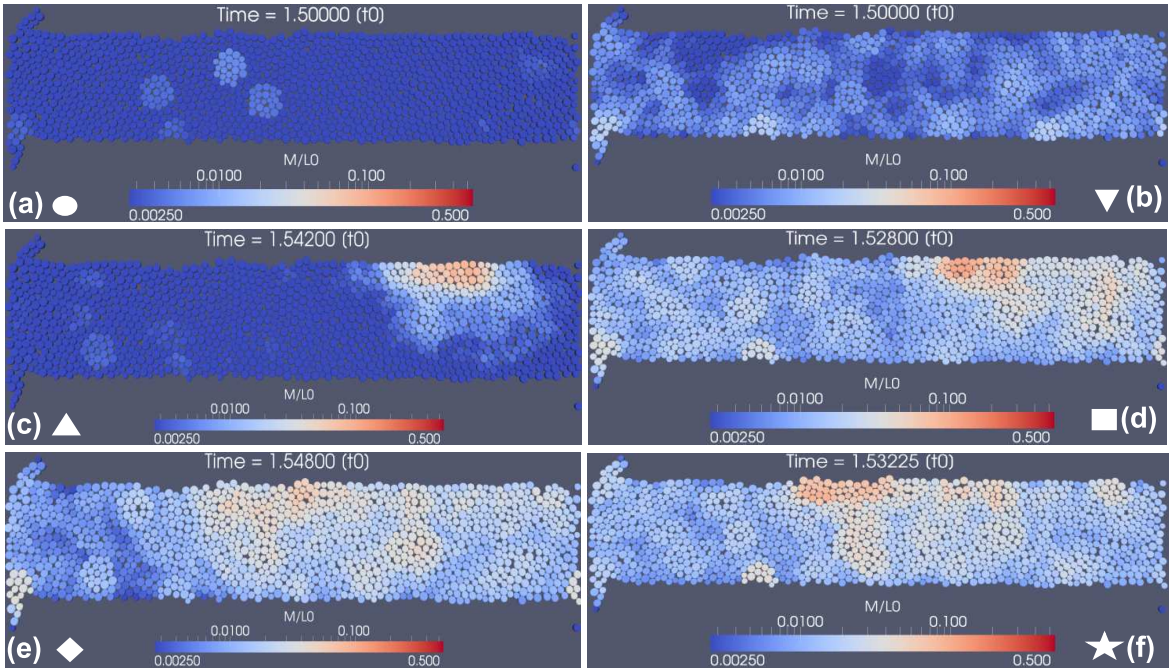

Fig. 3: (Color online) Non-affine deformation metric map, $M(\bar{r}, t)$, at different times (see corresponding identifying symbols in fig. 2). (a), (c), (e): reference run, without applied vibration. (b), (d), (f): with applied vibration. Only granular layer particles are visualized. Each particle is colored according to the logarithm of the local M value, with the color scale given below each plot. Corresponding animated movies are available as part of the Supplementary Materials (see footnote [1]), showing the temporal evolution of $M(\bar{r}, t)$ during the time interval $[1.46; 1.56]$, for both the reference and perturbed runs. Note that there are unbonded particles protruding from the granular layer on the left side of each plot. See sect. I of the Supplementary Materials (see footnote [1]) for information about them.

applied only within the time interval $[10.06; 10.16]$. We have also observed a similar effect in runs where vibration is applied multiple times in succession. However, in general we find that triggering is effective only when vibration is applied close to the failure time determined from the reference simulation (when the friction coefficient is between 50% and 90% of peak value observed in the reference run). AC vibration is not effective in triggering slip events when applied well before the failure time determined from the reference run.

Figure 2(b) shows that the stick periods following AC vibration are still accompanied by vertical dilation of the system. Slip events triggered by AC vibration result in compaction of the granular layer most of the time, with dilation in a few cases. However, we did not collect enough statistics of triggered slip events to determine whether AC vibration changes the fraction of compactant events *vs.* dilational ones.

Finally, fig. 2(e), gray line, shows that the average non-affine deformation, $\langle M(t) \rangle$, still signals the onset of slip, without a significantly different pattern compared to the reference run. However, looking at the spatial maps of $M(\bar{r}, t)$, at three different times during the AC perturbation interval, figs. 3(b), (d) and (f), we note that non-affine deformation is more widespread across the granular layer before the onset of slip. We believe that this wider distribution of non-affine deformation contributes to increasing the probability of triggering slip. The peak values of $M(\bar{r}, t)$ still occur mainly in a small area at the interface with the driving block bottom, during slip, as for the rerence run. As a slip event evolves, the local non-affine deformation becomes more uniform, fig. 3(f).

Conclusion. – We have performed 2D MD simulations of stick-slip in sheared granular layers with an elastic driving block driven at constant speed, which explores effects relevant for earthquakes and laboratory setups. We have compared runs without/with applied vibration, with the purpose of investigating dynamic triggering of slip events. We observe from our results that vibration can trigger the onset of slip events. These events unfold in much the same way as they do in the reference run. We have shown this result both at the macroscopic scale, recording the time evolution of the (normalized) shear stress upon the driving block, and at the mesoscopic scale, showing the temporal evolution of the spatial distribution of local non-affine deformation, $M(\bar{r}, t)$.

Another important result is the observation of widespread non-affine deformation prior to the onset of slip in the perturbed run. This is similar to the broad spatial deformation that occurs after the slip event in the reference run (fig. 2(e)), which illustrates that larger scale

particle-to-particle contact mobilization is occuring during applied vibration, a process that facilitates the occurence of slip events.

The metric M is useful for showing where and when non-affine strains develop, but it does not provide any information about why non-affine deformation occurs and which particle features affect it. Thus, future investigation is required to focus on identification of the different contributions of grain-scale mechanisms (rotation, frictional sliding, interlocking due to complex particle shape [25]) to the development of non-affine strains and on characterizing which of these mechanisms are more activated by elastic wave propagation through the granular layer. For example, Aharonov *et al.* showed with their 2D MD simulations that, prior to and during slip onset, the fraction of particle contacts in sliding mode increases exponentially for those contacts bearing a contact force smaller than the average value (weak contacts) [15]. The transition from static friction to dynamic friction for weak contacts may be accelerated in the presence of applied vibration, thus leading to a sudden increase in the number of sliding contacts in the neighborhood of the particles belonging to the force chains. This particle scale picture, if confirmed, may explain the concurrent rising of non-affine deformation at the onset of slip and suggests to investigate in the future whether force chain buckling [26] plays a major role also in dynamic triggering of slip events. This could potentially lead to a better understanding of the micromechanics of dynamic earthquake triggering.

Future studies will also address the role of macroscopic parameters and their role in controlling dynamic triggering in the double-axial shear configuration, *e.g.*, AC vibration amplitude, AC vibration frequency, σ_n and the substrate/driving block thickness. Similar investigations have been performed experimentally [27] and numerically [11,28] for traditional spring-slider systems. In addition, we will improve the statistics of dynamically triggered slip events. Improved statistics will allow us to assess if and how repeatedly applied AC pertubation changes the statistical properties of other macroscopic variables that are measured both in laboratory experiments and in the field, *e.g.*, slip stress drop/size and inter-event time, and allow for detailed comparisons with experiments and field observations of triggering.

* * *

We would like to thank H. J. Herrmann, L. de Arcangelis, E. Aharonov, L. Goren, L. Kondic and B. Ferdowsi for extensive discussions and S. Abe and D. Weatherley for support in developing our model using the `https://twiki.esscc.uq.edu.au/bin/view/ESSCC/ParticleSimulation` ESyS-Particle code. We acknowledge the support of the Swiss National Science Foundation (projects No. 206021-128754 and 200021-135492) and Institutional Support at the Los Alamos National Laboratory.

REFERENCES

[1] Gomberg J., Bodin P., Larson K. and Dragert H., *Nature*, **427** (2004) 621.
[2] Freed A., *Annu. Rev. Earth Planet. Sci.*, **33** (2005) 335.
[3] van der Elst N. and Brodsky E., *J. Geophys. Res.*, **115** (2010) B07311.
[4] Marone C., *Annu. Rev. Earth Planet. Sci.*, **26** (1998) 643.
[5] Mair K. and Marone C., *J. Geophys. Res.*, **104** (1999) 28899.
[6] Anthony J. and Marone C., *J. Geophys. Res.*, **110** (2005) B08409.
[7] Savage H. and Marone C., *J. Geophys. Res.*, **113** (2008) B05302.
[8] Johnson P., Savage H., Knuth M., Gomberg J. and Marone C., *Nature*, **451** (2008) 57.
[9] Place D. and Mora P., *J. Comput. Phys.*, **150** (1999) 332.
[10] Wang Y., Abe S., Latham S. and Mora P., *Pure Appl. Geophys.*, **163** (2006) 1769.
[11] Capozza R., Vanossi A., Vezzani A. and Zapperi S., *Phys. Rev. Lett.*, **103** (2009) 085502.
[12] Brown S. and Scholz C., *J. Geophys. Res.*, **90** (1985) 12575.
[13] Griffith W., Nielsen S., Toro G. D. and Smith S., *J. Geophys. Res.*, **115** (2010) B08409.
[14] Morgan J. and Boettcher M., *J. Geophys. Res.*, **104** (1999) 2703.
[15] Aharonov E. and Sparks D., *J. Geophys. Res.*, **109** (2004) B09306.
[16] Ciamarra M. P., Lippiello E., Godano C. and de Arcangelis L., *Phys. Rev. Lett.*, **104** (2010) 238001.
[17] Gomberg J. and Johnson P., *Nature*, **437** (2005) 830.
[18] Reynolds O., *Philos. Mag.*, **20** (1885) 469.
[19] Falk M. and Langer J., *Phys. Rev. E*, **57** (1998) 7192.
[20] Utter B. and Behringer R., *Phys. Rev. Lett.*, **100** (2008) 208302.
[21] Goldenberg C., Tanguy A. and Barrat J.-L., *EPL*, **80** (2007) 16003.
[22] Lemaitre A., *Phys. Rev. Lett.*, **89** (2002) 195503.
[23] Daub E. and Carlson J., *Phys. Rev. E*, **90** (2009) 066113.
[24] Tordesillas A., Muthuswamy M. and Walsh S., *J. Eng. Mech.*, **134** (2008) 1095.
[25] Pena A., McNamara S., Lind P. and Herrmann H., *Granular Matter*, **11** (2009) 243.
[26] Tordesillas A., Zhang J. and Behringer R., *Geomech. Geoeng. Int. J.*, **4** (2009) 3.
[27] Daniels K. E. and Behringer R. P., *Phys. Rev. Lett.*, **94** (2005) 168001.
[28] Melhus M. F., Aranson I. S., Volfson D. and Tsimring L. S., *Phys. Rev. E*, **80** (2009) 041305.